Underlying Mechanisms of Symmetric Calcium Wave Propagation in Rat Ventricular Myocytes

Saisunder Subramanian,* Sergej Viatchenko-Karpinski,† Valeriy Lukyanenko,† Sandor Györke,† and Theodore F. Wiesner*

*Department of Chemical Engineering, Texas Tech University, Lubbock, Texas 79409, and †Department of Physiology, Texas Tech University Health Science Center, Lubbock, Texas 79430 USA

ABSTRACT Calcium waves in heart cells are mediated by diffusion-coupled calcium-induced calcium release. The waves propagate in circular fashion. This is counterintuitive in view of the accepted ultrastructure of the cardiac myocyte. The density of calcium release sites in the transverse direction is four times higher than in the longitudinal direction. Simulations with release sites localized along Z-lines and isotropic diffusion yielded highly elliptical, nonphysiological waves. We hypothesized that subcellular organelles counteracted the higher release site density along the Z-lines by acting as transverse diffusion barriers and sites of active calcium uptake. We quantified the reduction of transverse diffusion by microinjecting cells with the nonreactive dye fluorescein. The ratio of the radial diffusion coefficient to the longitudinal coefficient was 0.39. Inhibition of mitochondrial uptake by rotenone accelerated the wave in the transverse direction. Simulations with release sites clustered at the Z-lines and a transverse diffusion coefficient 50% of the longitudinal coefficient generated waves of ellipticity 2/1 (major axis along the Z-line). Introducing additional release sites between the Z-lines at a density 20% of that on the Z-lines produced circular waves. The experiments and simulations support the presence of transverse diffusion barriers, additional uptake sites, and possibly intermediate release sites as well.

INTRODUCTION

Spontaneous calcium waves in cardiac myocytes have been implicated in pathologies such as arrhythmia, after-contractions, and depression of systolic and diastolic function (Stern et al., 1988; Takamatsu and Wier, 1990; Grouselle et al., 1991; Lakatta, 1992). The underlying mechanisms of calcium wave propagation are believed to include diffusion of the free calcium ion, coupled to calcium-induced calcium release from ryanodine-sensitive release channels in the sarcoplasmic reticulum (SR) (Fabiato, 1983; Jaffe, 1991; Engel et al., 1995; Cheng et al., 1996a; Lukyanenko et al., 1999). Yet these two processes by themselves may not account entirely for the propagation characteristics of calcium waves. Immunochemical and ultrastructural evidence indicates that SR Ca^{2+} release channels are localized in the junctional and corbular SR, which occur primarily at the level of Z-lines and t-tubules (Jorgensen et al. 1993; Franzini-Armstrong and Protasi, 1997). Therefore, cellular ultrastructure is likely to play a significant role in calcium wave propagation as well. Elucidating the role of ultrastructure in the formation of calcium waves is consequently important in understanding the physiology and pathophysiology of excitation-contraction coupling in the heart.

Recent theoretical studies in one-dimensional mathematical models predicted that calcium waves should display saltatory propagation characteristics, distinct from wave propagation in a continuous excitable medium (Bugrim et al., 1997; Keizer and Smith, 1998; Keizer et al., 1998). In addition to theoretical investigations, the spatio-temporal properties of calcium waves have been investigated experimentally to understand the propagation mechanisms. Lukyanenko and Györke (1999) subsequently demonstrated saltatory propagation experimentally. Takamatsu and Wier (1990) observed semicircular waves that propagated at a constant velocity typically equal to 100 μm/s. Ishide et al. (1990) reported circular waves in rat myocytes, which displayed fairly constant velocity, amplitude, and width during propagation. Williams et al. (1992) observed circular calcium waves that propagated at speeds of 50–150 μm/s. Engel et al. (1994) distinctly resolved calcium waves in rat cardiomyocytes into longitudinal and transverse components. Both components traveled at constant velocities ranging from 30–125 μm/s. A linear regression of multiple waves yielded an average longitudinal velocity of 79 μm/s and an average transverse velocity of 56 μm/s. Wussling and Salz (1996) described spherical waves reaching a maximum velocity of 113 μm/s, which appeared circular in two-dimensional images of rat ventricular myocytes. Taken together, these investigations characterize calcium waves spreading in directions both perpendicular to and parallel with the Z-lines, with the longitudinal velocity nearly the same or larger than the velocity parallel to a Z-line.

However, such wave velocities are counterintuitive in view of the known ultrastructure of the cardiac myocyte. The spacing of calcium release sites in the transverse direction is approximately 0.5 μm, whereas that in the longitudinal direction is ~2.0 μm. This arrangement has been established on the basis of two experimental approaches.

Received for publication 9 February 2000 and in final form 5 October 2000.

Address reprint requests to Dr. Theodore F. Wiesner, Texas Tech University, Department of Chemical Engineering, Box 43121, Lubbock, TX 79409. Tel.: 806-742-1448; Fax: 806-742-3552; E-mail: ted.wiesner@coe.ttu.edu.

0006-3495/01/01/01/11 $2.00

Fluorescent images of calcium sparks occur predominantly along the T-tubules (Shacklock et al., 1995; Parker et al., 1996). Electron microscopy has revealed the minimum spacing between calcium release units of 414 nm along the face of contact between T-tubules and junctional SR (Flucher and Franzini-Armstrong, 1996; Franzini-Armstrong, 1996; Franzini-Armstrong et al., 1999). Thus, the density of release sites in the transverse direction is apparently four times that in the longitudinal direction. Such an arrangement should give rise to elliptical waves oriented along the Z-lines, rather than the circular waves actually observed.

In the present study, we investigated what factors would cause calcium waves in cardiac myocytes to propagate symmetrically. It has been suggested that transverse diffusion is inhibited by the anisotropic arrangement in the myofibrillar space of diffusion obstacles, such as mitochondria, nuclei, the SR, contractile and elastic proteins, and the cytoskeleton (Engel et al., 1994; Wussling et al., 1997). To explain the paradoxical wave shape, we hypothesized that transverse diffusion barriers formed by the cytoplasmic organelles counteract the acceleration of wave velocity due to the higher release site density along the Z-lines. We simulated Ca sparks and their transition to waves with a two-dimensional mathematical model. The model includes spatial heterogeneities in release site location, anisotropic diffusion in the transverse and longitudinal directions, and the optical blurring effect of the confocal microscope. With release sites clustered along Z-lines and isotropic diffusion, we obtained waves much more elliptical than observed in vitro (major axis along the Z-line). Through microinjection of a nonreactive fluorophore, we found experimentally that the cytoplasm is indeed anisotropic from a diffusion standpoint, with longitudinal diffusion favored over transverse diffusion. We then found that the combination of release sites clustered at the Z-lines and a reduced transverse diffusion coefficient generated simulated waves of comparable ellipticity to those obtained via confocal microscopy in vitro.

Our experiments and simulations therefore indicate that diffusional anisotropy, as well as diffusion-coupled calcium-induced calcium release, is a major determinant of wave propagation characteristics in cardiac myocytes. We discuss the physiological significance of cytoplasmic heterogeneity and possible implications for the presence of release sites not localized along the Z-lines.

MATERIALS AND METHODS

Geometric model

To simulate Ca^{2+} waves, we constructed an approximate geometric model of a half-sarcomere with spatially discrete release sites (Fig. 1). The geometry of the model includes the diadic cleft and the sarcomere outside the cleft after Peskoff and Langer (1998). We used cylindrical coordinates *(r, x)* with the planes of the Z-lines at $x = 0$, 2 μm, 4 μm, etc. The *x*-axis lies along the longitudinal axis of the cell. In the simulation domain there are 50 individual release sites (equally spaced at intervals of 0.5 μm) along the radial direction, located at Z-lines spaced 2 μm apart. Additional intermediate release sites are placed between adjacent Z-lines in some of the simulations.

Mathematical model

To understand the mechanism of symmetric Ca^{2+} wave propagation, it was important to use at least a two-dimensional model of the sarcomere. The mathematical model includes release flux from discrete release sites, spatially homogeneous removal fluxes (SR Ca^{2+} pumps and soluble buffers), diffusible dye, the diffusible Ca^{2+}:dye complex, and spatially homogeneous endogenous buffers. Simulations were run for different cases by varying the isotropy of diffusion and release site spacing. Values for the diffusion coefficient of free Ca^{2+} range from 100 $\mu m^2/s$ (Langer and Peskoff, 1996) to 600 $\mu m^2/s$ (Pratusevich and Balke, 1996). We used a value of 300 $\mu m^2/s$ (Albritton et al., 1992) as a standard value for the diffusion coefficient of free calcium ion (D_{Ca}) and an apparent diffusion coefficient for both the free and bound indicator (D_{dye}, $D_{Ca:dye}$) of 20 $\mu m^2/s$ (Harkins et al., 1993). The spatio-temporal concentrations of the free cytoplasmic calcium (Ca) and the Ca:dye complex (Ca:dye) and the temporal evolution of bound buffer concentration (Ca:B) were described by the following coupled system of equations.

$$\frac{\partial[\mathrm{Ca}]}{\partial t} = \frac{D_{\mathrm{Ca,r}}}{r}\frac{\partial}{\partial r}\left(r\frac{\partial[\mathrm{Ca}]}{\partial r}\right) + D_{\mathrm{Ca,x}}\frac{\partial^2[\mathrm{Ca}]}{\partial x^2} + q_{\mathrm{rel}} - q_{\mathrm{rem}} + q_{\mathrm{rel0}} \quad (1)$$

$$\frac{\partial[\mathrm{Ca{:}dye}]}{\partial t} = \frac{D_{\mathrm{Ca:dye,r}}}{r}\frac{\partial}{\partial r}\left(r\frac{\partial[\mathrm{Ca{:}dye}]}{\partial r}\right) + D_{\mathrm{Ca:dye,x}}\frac{\partial^2[\mathrm{Ca{:}dye}]}{\partial x^2} + q_{\mathrm{dye}} \quad (2)$$

$$\frac{d[\mathrm{Ca{:}B}]}{dt} = q_{\mathrm{b}} \quad (3)$$

Here $D_{i,j}$ is the diffusion coefficient of species i in direction j, q_{rel} is the release flux, q_b is the buffering flux, and q_{rem} is the removal flux. The removal flux consists of three contributions:

$$q_{\mathrm{rem}} = q_{\mathrm{b}} + q_{\mathrm{SR}} + q_{\mathrm{dye}} \quad (4)$$

The quantity q_b is removal by binding to endogenous buffers, and q_{SR} is the removal by the Ca^{2+} ATPase of the SR reticulum. q_{dye} is the binding flux of free calcium to the indicator dye. The quantity q_{rel0} is the calcium release from the SR under basal conditions. Removal by the Ca^{2+} ATPase and Na^+/Ca^{2+} exchanger of the sarcolemma (SL) is neglected in this study because of its minor role in regulating Ca^{2+} transients in rat ventricular myocytes (Balke et al., 1994).

The Ca^{2+} release flux, q_{rel}, triggered at each release site was implemented using an extension of the fire-diffuse-fire model presented recently by Keizer et al. (1998, Appendix, Eqs. 7–10):

$$q_{\mathrm{rel}}(r,t) = \begin{cases} q_0 e^{-t/\tau}, & \text{if } r = \text{a trigger site} \\ \nu_{\mathrm{rel}} f_0[\mathrm{Ca}(r,t)][\mathrm{Ca_{SR}} - \mathrm{Ca}(r,t)], & \text{if } \mathrm{Ca}(r,t) \geq c^* \\ & \text{and } r = \text{nontrigger release site} \\ 0, & \text{otherwise} \end{cases} \quad (5)$$

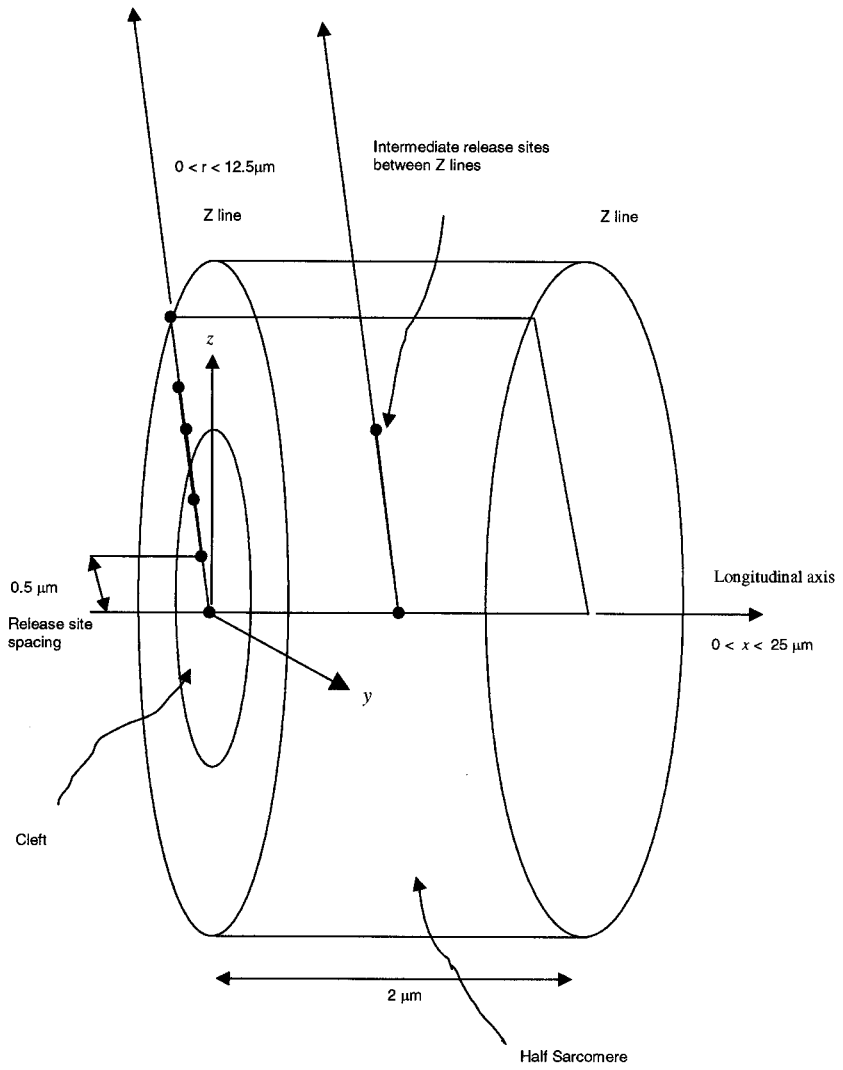

FIGURE 1 Geometry of the model. The diadic cleft and sarcomere are modeled in cylindrical coordinates (r, x). The simulation was conducted in a domain including a distance of 25 μm in both the r and x directions. Discrete release sites of identical source strength are placed at a distance of 0.5 μm from each other in the r direction, at each Z-line. The Z-lines are spaced 2 μm apart along the longitudinal direction. Intermediate release sites are placed (one intermediate site for every five release sites at Z-lines) between Z-lines in some of the simulations to study their effect of wave symmetry and velocity. We obtained the distribution of Ca:dye at various times in this simulation domain in the form of r-x images .

To initiate wave propagation, we provided three trigger release sites (a circular trigger region of radius 1.5 μm) having an exponentially decaying release flux. The magnitude of the trigger calcium was $q_0 = 15$ mM/s, with a decay constant $\tau = 2$ ms. For release at nontrigger sites, the coefficient ν_{rel} is the conductance of the release site; and $f_0[\mathrm{Ca}(r,t)]$ is the calcium-dependent fractional activation of each site. $\mathrm{Ca}(r,t)$ is the local free calcium concentration. The quantity c^* is the threshold value of myoplasmic calcium, above which the site releases calcium.

$\mathrm{Ca_{SR}}$ is the calcium concentration in the sarcoplasmic reticulum. Increased SR calcium content has been shown to increase the magnitude of calcium release and enhance wave propagation. When basal calcium levels are maintained at a high level via manipulating membrane potential, calcium waves occurred at a significantly higher frequency and velocity than when low basal calcium is maintained (Takahashi and Takamatsu, 1997). It is these spontaneous waves that are likely significant from a pathological standpoint. With conditions of overload, caffeine-evoked waves propagate without significant decay in either amplitude or velocity (Trafford et al., 1995). Nuclear magnetic resonance studies have shown that upon increasing the cellular Ca^{2+} load, lumenal Ca^{2+} can rise up to 5 mM (Cheng et al. 1996a). Therefore we simulated calcium overload by setting $\mathrm{Ca_{SR}}$ to the constant value of 5 mM in all simulations.

With regard to the binding of calcium to endogenous buffers, its flux was calculated from the following equation, which lumps all the buffers into a single immobile pool:

$$q_b = k_{b,on}[\mathrm{Ca}][\mathrm{B}] - k_{b,off}[\mathrm{Ca{:}B}] \tag{6}$$

The rate constants for binding and dissociation are given by $k_{b,on}$ and $k_{b,off}$ respectively. [B] is the concentration of the free buffer at any time, and [Ca:B] is the concentration of the calcium-buffer complexes. The flux of calcium binding to the indicator is given by a similar expression:

$$q_{dye} = k_{dye,on}[\mathrm{Ca}][\mathrm{dye}] - k_{d,off}[\mathrm{Ca{:}dye}] \tag{7}$$

The quantity [dye] is the concentration of unbound indicator. This concentration and that of the unbound buffer [B] may be calculated from the following conservation relations:

$$[\mathrm{dye}] = [\mathrm{dye_T}] - [\mathrm{Ca{:}dye}] \tag{8}$$

$$[\mathrm{B}] = [\mathrm{B_T}] - [\mathrm{Ca{:}B}] \tag{9}$$

$[B_T]$ is the total concentration of buffers, and [dyeT] is the total concentration of indicator. This conservation relation among the total species, bound species, and free species holds when the initial distribution of the

TABLE 1 Parameters of the mathematical model of the Ca^{2+} wave:

Parameter	Value	Source
Diffusion		
$D_{Ca,x}$ ($\mu m^2\ ms^{-1}$)	0.30	Albritton et al., 1992
$D_{Ca\text{-}dye,x}$ ($\mu m^2\ ms^{-1}$)	0.02	Harkins et al., 1993
$D_{Ca,r}/D_{Ca,x}$	1, 0.5, 0.35	Variable simulation parameter
Ca^{2+} resequestration by SR		
V_{SR} ($\mu M\ s^{-1}$)	1000	Tang and Othmer, 1994
K_{SR} (nM)	120	Tang and Othmer, 1994
n	4.0	Lukyanenko et al., 1999
Ca^{2+} buffering		
$k_{b,on}$ ($nM^{-1}\ ms^{-1}$)	10^{-4}	Sipido and Wier, 1991
$k_{b,off}$ (ms^{-1})	4×10^{-2}	Sipido and Wier, 1991
$k_{d,on}$ ($nM^{-1}\ ms^{-1}$)	2.4×10^{-4}	Escobar et al., 1995
$k_{d,off}$ (ms^{-1})	1.8×10^{-2}	Escobar et al., 1995
K_D (nM)	740	Escobar et al., 1995
B_0 (nM)	2.50×10^5	Variable simulation parameter
Basal and threshold concentrations		
$[Ca_0]$ (μM)	0.1	Standard value
$[Ca{:}dye_0]$ (μM)	5	Initial steady-state value
$[dye_T]$ (nM)	5×10^4	Experimental value
$[Ca_{SR}]$ (mM)	5	Cheng et al., 1996a
c^* (μM)	1.5–3.5	Variable simulation parameter
PSF of confocal microscope		
σ_x (μm)	0.115	Pratusevich and Balke, 1996
σ_r (μm)	0.0289	Pratusevich and Balke, 1996
N (μm^{-3})	1870	Izu et al., 1998

buffer or dye is uniform and the diffusion coefficients of the free and bound species are the same.

The flux transported by the Ca^{2+} pumps was calculated from the expression given by Tang and Othmer (1994):

$$q_{SR} = \frac{V_{SR}Ca^n}{K_{SR}{}^n + Ca^n} \tag{10}$$

V_{SR} is the maximal pump capacity, K_{SR} is the calcium capacity at which the transport is half-maximal for a particular process, and n is the Hill coefficient. The term q_{rel0} represents basal leak and is given by

$$q_{rel0} = \frac{V_{SR}Ca_0{}^n}{K_{SR}{}^n + Ca_0{}^n} \tag{11}$$

Ca_0 is the basal calcium concentration, taken to be 100 nM. The parameters of release, diffusion, buffering, and uptake of Ca^{2+} were chosen from an accepted range of values in the literature after doing a parameter sensitivity analysis to obtain physiologically meaningful dimensions of Ca^{2+} sparks and waves. The parameters are presented in Table 1. The coupled system of equations was solved numerically using an interior collocation technique (Villadsen and Stewart, 1967; Segall and MacGregor, 1984.). The resulting system of ordinary differential equations (ODEs) was solved using the standard FORTRAN ODE solver LSODE. The solution was subject to the following initial and boundary conditions:

$$Ca(r,x,0) = Ca(0,0,t) = Ca(a,b,t) = Ca_0 \tag{12}$$

$$Ca{:}dye(r,x,0) = Ca{:}dye(0,0,t) = Ca{:}dye(a,b,t) = Ca{:}dye_0 \tag{13}$$

$$Ca{:}B(0) = \frac{Ca_0}{\frac{k_{b,off}}{k_{b,on}} + Ca_0} = Ca{:}B_0 \tag{14}$$

where $a = 25\ \mu m$ and $b = 25\ \mu m$ are the radial and longitudinal dimensions of the simulation domain, respectively. The simulations were run over a time domain of 0.3 s. The entire numerical routine was coded using AIX FORTRAN F90 (IBM Corp., Armonk, NY) and run in serial mode on an IBM SP 6000 (typical simulation run time of 25 min).

Model of point spread function

In confocal microscopy, the exact location of the wave front can be difficult to determine because of optical distortion. Experimental observation of the sawtooth pattern of wave propagation predicted by the theory is difficult due to the limited spatial resolution of confocal microscopy (Lukyanenko et al., 1999).

We simulated optical blurring of the confocal microscope by convolving the numerical solution of the Ca:dye concentration with a two-dimensional Gaussian model of the point spread function (PSF) of the confocal microscope (Izu et al., 1998).

$$PSF(r,x) = N \exp\left(-\frac{r^2}{\sigma_r{}^2}\right) \exp\left(-\frac{x^2}{\sigma_x{}^2}\right) \tag{15}$$

The quantity $N = (\sigma_r{}^2\sigma_x\pi^{3/2})^{-1}$, which normalizes the integral of the PSF over all space to unity. The standard deviations are taken in the range predicted in literature (Pratusevich and Balke, 1996) as shown in Table 1. The convolution was carried out by taking the product of the two-dimensional discrete Fourier transforms of the original signal and the PSF and then taking an inverse transform to obtain the simulated blurred image in IDL software (Research Systems, Boulder, CO).

Experiments

Cell isolation and confocal microscopy

Adult Sprague-Dawley rats (200–300 g) were euthanized by lethal injection of Nembutal (100 mg/kg), and single ventricular myocytes were

obtained by enzymatic dissociation as described previously (Györke et al., 1997). Experiments were performed using a Bio-Rad laser scanning confocal system (MRC 1024ES, Bio-Rad Laboratories, Hercules, CA) equipped with an Olympus 60 × 1.4 N.A. objective. The cells were loaded with Fluo-3 by a 20-min incubation with 5 μM Fluo-3/AM (acetoxymethyl ester form, Molecular Probes, Eugene, OR) at room temperature. Fluo-3 was excited by light at 488 nm (25 mW argon laser, intensity attenuated to 0.3%), and fluorescence was measured at wavelengths of >515 nm.

Wave generation studies

All experiments began in a bathing solution containing 1 mM Ca^{2+}. The standard Tyrode solution contained (in mM): 140 NaCl, 4 KCl, 0.5 $MgCl_2$, 1 or 10 $CaCl_2$, 10 Hepes, 0.25 NaH_2PO_4, 5.6 glucose, pH 7.3. All chemicals were from Sigma (St. Louis, MO) unless otherwise specified. Only cells lacking spontaneous Ca^{2+} oscillations were selected for further measurements. To initiate the calcium waves, the SR Ca^{2+} load was increased by elevating the extracellular calcium ($[Ca^{2+}]_o$) from 1 to 5 mM. All experiments were performed at room temperature (21–23°C). Images were acquired in the *x-y-t* scan mode of the microscope (pixel size, 0.419 μm; collection cycle time, ~120 ms) at a rate of 0.5 ms per scan. Image processing and analysis were performed by using NIH Image (National Institutes of Health, Bethesda, MD).

Passive diffusion studies

For passive diffusion studies, 1 mM fluorescein (sodium salt, Sigma) was added to the standard pipette solution. We used a combination of the confocal microscope system described above and the standard patch-clamp method described by Hamill et al. (1981). All patch-clamp experiments were performed at room temperature. Pipettes (2–4 MΩ) were made on a P-97 Universal Puller (Sutter Instruments, Novato, CA) from 1.5-mm borosilicate glass capillaries. Data were acquired using an Axopatch 200B amplifier and PCLAMP 5 software (Axon Instruments, Foster City, CA). *x-y* images (256 × 256 or 512 × 512 pixels) were recorded immediately after the whole-cell configuration was established, at a rate of one image per second. For image analysis, we used Scion Image (Scion Corp., Frederick, MD).

RESULTS

A temporal sequence of images in Fig. 2 illustrates a single propagating calcium wave in a single myocyte. A calcium spark ($t = 0$ ms) triggers a wave that propagates as an ever-expanding circle (117 ms $\leq t \leq$ 468 ms). At later times (585 ms $\leq t \leq$ 819 ms), the wave becomes distorted upon collision with the sarcolemma. Also visible at the later times is the fact that the highest concentration of Ca:dye lies at the leading edge of the wave, whereas the fluorescence at the center of the wave returns to a near-basal level.

As mentioned in the introduction, calcium release sites in cardiac myocyte are localized along the Z-lines. We simulated this arrangement by placing release sites 0.5 μm apart on planes separated by 2 μm (corresponding to Z-lines). In case I, the ratios of the radial to the longitudinal diffusion coefficients for all diffusing species were set equal to 1 (isotropic diffusion). The threshold for release site activa-

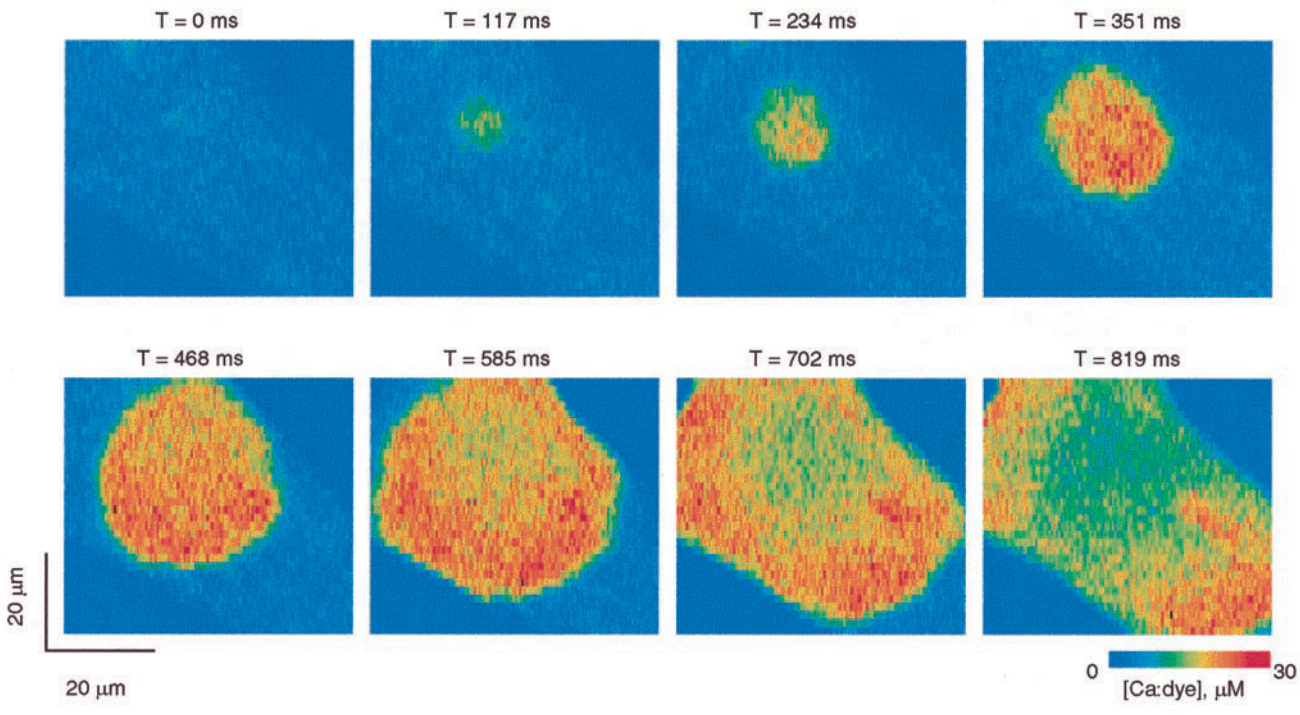

FIGURE 2 Experimental images showing symmetric calcium wave propagation. A representative series of images shows propagation of a Ca^{2+} wave with time. Pixel size is 0.419 μm; collection cycle time was 117 ms and the time to scan each line of the image was 0.5 ms. Calibration bars, 20 μm. $[Ca^{2+}]$ in the bathing solution was 5 mM. The cell longitudinal axis is 135° to the *x*-axis of the image. The velocity of the wave is essentially the same in all directions and is nearly constant (37 μm/s to 39 μm/s) from 234 ms to 468 ms.

tion (c^*) was set as 3.5 μM. The simulation results are illustrated in Fig. 3. The wave spread only in the transverse direction and would not propagate in the longitudinal direction even to the adjacent Z-lines (denoted by the columns of white dots). The simulated wave velocity along the Z-line (417 μm/s) is also much higher than seen in our experiments (~38 μm/s, Fig. 2). In one-dimensional wave models with a release site spacing of 2 μm, it has been seen that self-sustaining waves failed to materialize for thresholds >1.3 μM (Lukyanenko et al., 1999). However, with the increased density of release site spacing in this model, unrealistically high wave velocities resulted even for release thresholds as high as 3.5 μM. Clearly isotropic diffusion in conjunction with release sites localized along Z-lines cannot adequately explain the symmetric nature of the waves.

Intuitively, for the waves to be symmetric the diffusion will have to be anisotropic; i.e., diffusion in the transverse direction must be slower than in the longitudinal direction. Experimental studies of calcium sparks in calcium myocytes indicate that longitudinal diffusion of the calcium-dye complex is favored over transverse diffusion. A 50% reduction in the transverse diffusion coefficient has been shown to simulate (Smith et al., 1998) the experimentally observed ellipticity of 20% in Ca^{2+} sparks (Cheng et al., 1996a). Parker et al. (1996) quantitatively analyzed sparks obtained in cardiac myocytes by transverse and longitudinal confocal scans. They found that the fluorescent signal spread more slowly in the transverse scans. Employing the methods of Yao et al. (1995), they calculated the longitudinal diffusion coefficient of the calcium-dye complex as 17.1 μm/s, whereas that in the transverse direction as 7.9 μm/s. This yields a ratio of $D_{\text{transverse}}/D_{\text{longitudinal}} = 0.46$.

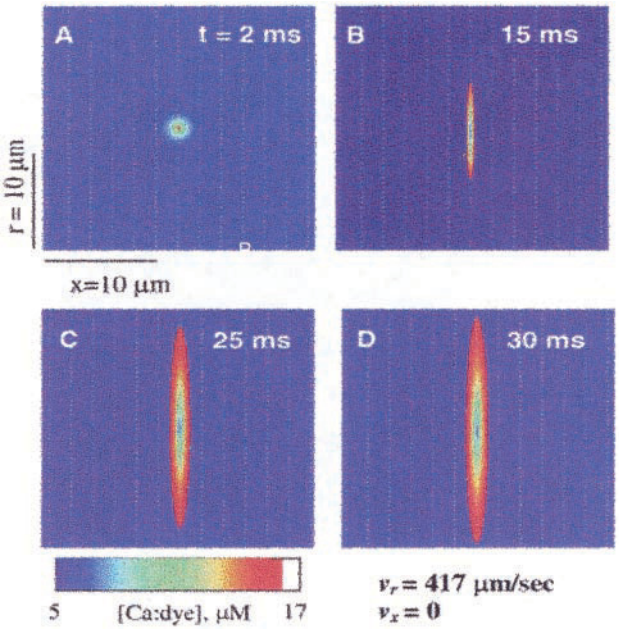

FIGURE 3 Case I: asymmetric Ca^{2+} wave propagation in an isotropic diffusion medium with release sites placed at Z-lines only. (*A–D*) *r-x* images illustrating asymmetric wave propagation at times t = 2, 15, 25, and 30 ms, respectively. The diffusion in this case is isotropic in the radial and longitudinal directions ($D_{Ca,r}/D_{Ca,x} = D_{Ca:dye,r}/D_{Ca:dye,x} = 1.0$) and release sites (represented by white dots) are placed at Z-lines only. The wave was triggered with an exponentially decaying release flux of magnitude q_0 = 15 mM/s and a decay constant of 2 ms over a region of radius 1.5 μm (three release units). The threshold of release activation at each site was 3.5 μM. The wave propagated to a distance of 25 μm in the radial direction but did not propagate to even the adjacent Z-lines (<2 μm) in the longitudinal direction. Wave velocities obtained were much higher (up to 417 μm/s) than the physiologically meaningful range of experimental wave velocities (30–125 μm/s).

To obtain a quantitative estimate of this anisotropy without the complications of reactions among the diffusing species, we investigated passive diffusion in the myocyte using the nonreactive dye fluorescein. Fluorescein (sodium salt, Sigma) is a fluorescent organic compound of low molecular weight (376.5) with minimal binding affinity. For short time scales, diffusion of fluorescein should dominate any nonspecific binding by it to cellular constituents. Therefore its spatiotemporal distribution in the myocyte should be a reasonable marker of intrinsic diffusional anisotropy.

One can compute the ratio of the radial diffusion coefficient to the longitudinal diffusion coefficient by measuring the extents of diffusion in the transverse and longitudinal directions. The myocyte may be considered as a cylinder with radially symmetric diffusion properties but having a longitudinal diffusion coefficient that differs from the radial diffusion coefficient. The transport of fluorescein in the cell can then be modeled with an unsteady diffusion equation in a semi-infinite, anisotropic medium with an instantaneous point source on its surface. (Such a model neglects the curvature of the cell membrane at the patch pipette and is valid only until the wave contacts the sarcolemma at the ends of the cell.). From the analytical solution to this model (Carslaw and Jaeger, 1959; Deen, 1998), one can derive the following relationship:

$$\frac{D_r}{D_x} \propto \left(\frac{y'}{x'}\right)^2 \tag{16}$$

The quantities D_r and D_x are the radial and longitudinal diffusion coefficients, respectively. The apparent extents of diffusion y' and x' lie in the confocal plane, in the transverse and longitudinal directions, respectively. The ratio of apparent extents is proportional to the ratio of extents at any confocal plane, because of the symmetry of the solution of the diffusion equation. Therefore the estimate is insensitive to out-of-focus scanning. The ratio of extents of diffusion is also independent of time. Thus this estimate of the ratio of diffusion coefficients is very robust. Because of the uncertainties of the focal plane relative to the plane in which the dye is injected, however, this method cannot be used to determine absolute values of the diffusion coefficients.

An example of the differing extents of diffusion is illustrated in Fig. 4 *A*. After 10 s, the fluorescein has diffused 7.3 μm (x') longitudinally and 5.2 μm (y') transversely. By Eq. 16, the

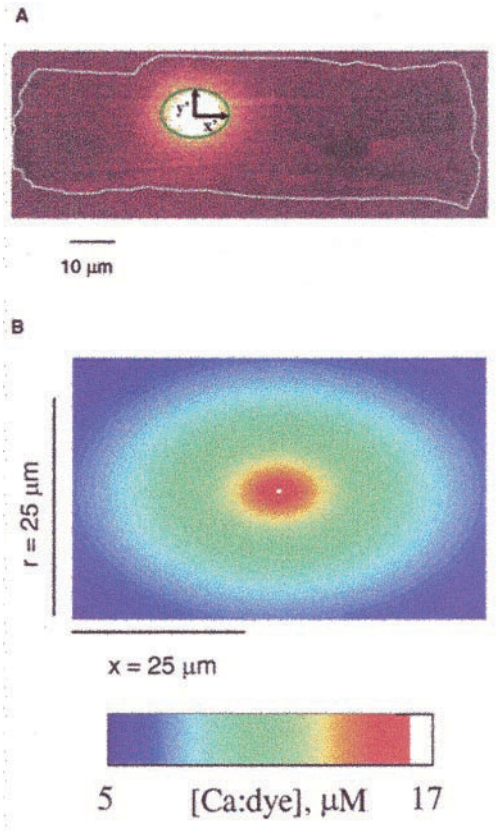

FIGURE 4 Comparison of experimental diffusion of fluorescein and simulated diffusion in an excitable and nonexcitable media. (*A*) *y-x* experimental image showing anisotropic diffusion of fluorescein in an isolated cardiac myocyte. The cell boundaries are outlined. After 10 s, the dye has diffused 7.3 μm (x') longitudinally and 5.2 μm (y') transversely (elliptical outline). (*B*) *r-x* image showing passive diffusion of fluo-3 (D_{dye} = 0.02 $\mu m^2\ ms^{-1}$) from a point source of concentration 20 μM. All the pumps and buffers were disabled in this simulation and all release sites were inactivated. The diffusion coefficient in the radial direction was set to 50% of that in the longitudinal direction. The ellipticity of the simulated fluorescence ($y'/x' = 0.72$) compared favorably with the experimental ellipticity in Fig. 4 *A* ($y'/x' = 0.71$). The qualitative similarity of images *A* and *B* suggested that a diffusion coefficient ratio of 0.50 was a reasonable mimic of the experimentally observed anisotropy.

ratio of the radial to the longitudinal diffusion coefficient is $D_r/D_x = 0.50$. From such measurements in 10 different myocytes, we obtained an average value of $D_r/D_x = 0.39 \pm 0.14$.

Using the results of our own fluorescein experiments as well as the calculated diffusion coefficients from the spark studies of Parker et al. (1996), we conservatively set $D_{dye,r}/D_{dye,x} = 0.5$. We then simulated the passive diffusion of fluo3 ($D_{dye,x} = 0.02\ \mu m^2\ ms^{-1}$) from a point source of concentration 20 μM (Fig. 4 *B*). To ensure that the diffusing species was unreactive, all pumps, buffers, and release sites were inactivated. The ellipticity of the simulated fluorescence ($y'/x' = 0.72$) compared favorably with the experimental ellipticity in Fig. 4 *A* ($y'/x' = 0.71$). The qualitative similarity of images *A* and *B* suggested that a diffusion coefficient ratio of 0.5 was a reasonable mimic of the experimentally observed diffusional anisotropy.

We then restored the excitable medium by reactivating the pumps, buffers, and release sites (Fig. 5) and examined the effects of reduced radial diffusion on the shape of calcium waves. We fixed the values of the longitudinal diffusion coefficients as in Table 1($D_{Ca,x} = 0.30\ \mu m^2\ ms^{-1}$, $D_{Ca:dye,x} = 0.02\ \mu m^2\ ms^{-1}$), while setting $D_{Ca,r}/D_{Ca,x} = D_{Ca:dye,r}/D_{Ca:dye,x} = 0.5$. All other simulation parameters were kept the same as in Fig. 3. In contrast to the situation of isotropic diffusion, reduced radial diffusion resulted in saltatory propagation of waves longitudinally across two additional Z-lines. The ellipticity of the waves compared more favorably than in case I to the experiment in Fig. 2. The radial wave velocities (up to 120 μm/s) dropped to the upper end of the physiologically meaningful range of experimental wave velocities (30–125 μm/s). However, the wave still propagated faster in the radial direction. The ellipticity of this wave was 2/1, as measured by the ratio of radial wave velocity to longitudinal wave velocity. Only

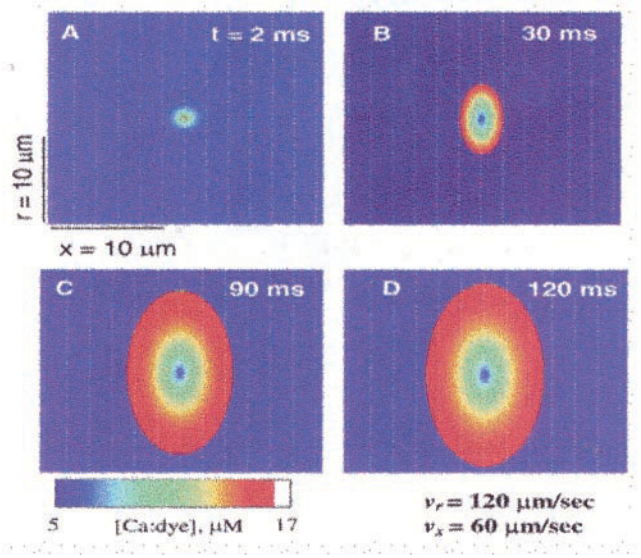

FIGURE 5 Case II: asymmetric Ca^{2+} wave propagation in an anisotropic diffusion medium with release sites placed at Z-lines only. (*A–D*) *r-x* images illustrating asymmetric wave propagation at times t = 2, 30, 90, and 120 ms, respectively. The diffusion in this case is anisotropic in the radial and longitudinal directions ($D_{Ca,r}/D_{Ca,x} = D_{Ca:dye,r}/D_{Ca:dye,x} = 0.5$) and release sites (represented by white dots) are placed at Z-lines only. The wave was triggered with an exponentially decaying release flux of magnitude q_0 = 15 mM/s and a decay constant of 2 ms over a region of radius 1.5 μm (three release units). The threshold of release activation at each site was 3.5 μM. The increased density of release site spacing in the transverse direction reverses the asymmetry (opposite to that in 4 *B*) and the wave propagates faster in the transverse direction, although the ratio of diffusion coefficients is the same as in 4 *B*. Anisotropic diffusion with the radial-longitudinal diffusion coefficient ratios at 0.50 alone was not sufficient to account for symmetric wave propagation. However, diffusion is faster in the longitudinal direction than observed in case I (Fig. 3). Wave velocities obtained (120 μm/s) are now in the upper end of the physiological range (30–125 μm/s).

with unrealistically low ratios of $D_{Ca,r}/D_{Ca,x}$ did the wave velocities approach each other (simulations not shown). These ratios were deemed unrealistic because of the characteristics of fluorescein diffusion given in Fig. 3. Thus anisotropic diffusion alone was not sufficient to yield symmetric wave propagation.

We next explored what additional factors would yield circular waves (ellipticity ~1), with velocities closer to the physiological range. Intuitively, increasing buffer concentrations should reduce wave velocities. It has been shown that Ca^{2+} release could propagate along restricted spaces such as between mitochondria and myofilaments, with Ca^{2+} buffering capacity exerting a critical influence on this type of Ca^{2+} movement (Kargacin, 1994). However, a parametric study of buffering on wave velocities indicated that velocities remained high even at a buffering capacity of 250 μM (simulations not shown).

In our previous experimental and modeling studies, diffusion-coupled calcium-induced calcium release alone has been shown to be inadequate in generating propagating waves (Lukyanenko et al., 1999). A possible potentiator of waves is increased sensitivity of the Ca^{2+} release channel to lumenal Ca^{2+}. We mimicked the increase in sensitivity in the model by lowering the threshold of ryanodine receptor activation. This, however, resulted in increased wave velocities and showed comparable effects in both directions.

We next investigated the role that additional release sites between the Z-lines may play in wave formation. The sites may be present in regions of close apposition between the junctional SR (jSR) and the sarcolemma (Jorgensen et al., 1985), or axial tubules of the transverse-axial tubular system (Forbes and Van Niel, 1988; Ogata and Yamasaki, 1993). To enhance the propagation velocity in the longitudinal direction, we introduced additional release sites between Z-lines at a 1-μm distance. As can be seen in Fig. 6, the waves propagated symmetrically under these conditions. A density ratio of one intermediate release site for every five release sites at a Z-line was found to be adequate to reach wave velocities comparable in both radial and longitudinal directions. The ellipticity of the simulations compare very favorably to the symmetric waves seen in experiments (Fig. 2). The magnitudes of the wave velocities now lie at the upper end of the physiological range (Fig. 6, *A–D*), and the simulated waves feature a ring-like appearance. Also similar to experiments is the fact that the highest fluorescence level is at the leading edge of the wave (Fig. 6 *E*). However the simulated peak Ca:dye levels, although in the same order of magnitude, are ~50% of the experimental values. We later discuss the quantitative reconciliation of our model with our experiments.

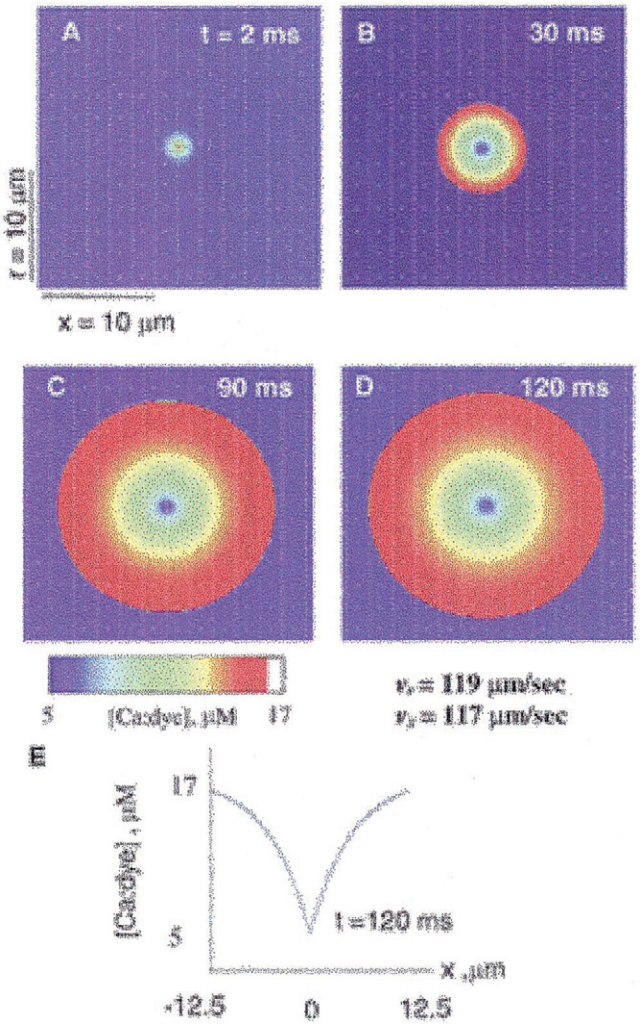

FIGURE 6 Case III: symmetric Ca^{2+} wave propagation in an anisotropic diffusion medium with release sites placed between Z-lines. (*A–D*) *r-x* images illustrating symmetric wave propagation at times t = 2, 30, 90, and 120 ms, respectively. The diffusion in this case is anisotropic in the radial and longitudinal directions ($D_{Ca,r}/D_{Ca,x}$ = 0.50) and release sites (represented by white dots) are placed at Z-lines with additional release sites between Z-lines at the rate of one intermediate release site for every five release sites at an adjacent Z-line. The wave was triggered with an exponentially decaying release flux of magnitude q_0 = 15 mM/s and a decay constant of 2 ms over a region of radius 1.5 μm (three release units). The threshold of release activation at each site was 3.5 μM. The wave propagated symmetrically to almost equal distances (~10 μm) in either direction. E, elevation of Ca:dye concentration in the simulated wave at t = 120 ms. The peak concentration of the wave is at the leading edge.

DISCUSSION

Extensive experimental research over the past 10 years has illustrated the nature of calcium waves in cardiac myocytes (Takamatsu and Wier, 1990; Ishide et al., 1990; Williams et al., 1992; Cheng et al., 1994, 1996a; Engel et al., 1994, 1995; Trafford et al., 1995; Wussling and Salz, 1996; Wussling et al., 1997; Failli et al., 1997; Lukyanenko et al., 1999; Lukyanenko and Györke, 1999). Separate and parallel research into the underlying mechanisms of calcium waves has been primarily theoretical in nature (Stern, 1992; Bugrim et al., 1997; Kupferman et al., 1997; Izu et al., 1998; Keizer and Smith, 1998; Keizer et al., 1998; Peskoff and

Langer, 1998; Dawson et al., 1999). The theoretical studies have often involved significant simplifications in the governing equations to obtain mathematically tractable solutions. These simplifications typically include reducing the geometry to a single spatial dimension, applying the fast buffering approximation (Wagner and Keizer, 1994), and assuming that the cytosolic calcium concentration is much less than the K_D values of the buffers (Koch, 1999). This reduces the system of coupled nonlinear reaction-diffusion equations to a single linear partial differential equation. The present study relaxes these three assumptions. Our numerical model incorporates the current theories of calcium wave propagation and, with simulations complementing experiments, indicates that the characteristics of calcium wave propagation are highly dependent upon cell ultrastructure.

Because of the known myocyte ultrastructure and the observed saltatory spark-to-wave transition, we felt it was important to include discrete release in the model. There is strong experimental evidence that the distribution of release sites is highly organized in a discrete fashion in the cardiac myocyte (Shacklock et al., 1995; Flucher and Franzini-Armstrong, 1996; Parker et al., 1996; Franzini-Armstrong, 1996; Franzini-Armstrong et al., 1999). It is now accepted that calcium waves result from the spatial and temporal summation of calcium sparks. For slowly propagating waves, or waves in the presence of EGTA, discrete calcium release events, similar to sparks, can be detected in the wave front. The discrete events appear to recruit other sparks in the wave front, so that the wave progresses in a saltatory manner (Cheng et al., 1996a; Lukyanenko and Györke, 1999). This mechanism is known as fire-diffuse-fire. Such a model shows that sparks can merge into saltatory waves (Keizer and Smith, 1998; Dawson et al., 1999).

Published theoretical work differs on the significance of discrete release. Studies by Kupferman et al. (1997) indicate that discrete channels introduce only small corrections to a model in which calcium is released uniformly from the surface of the intracellular stores. On the other hand, the simulations of Bugrim et al. (1997) indicate that a heterogeneous distribution of calcium release channels heavily influences propagating characteristics of calcium waves. Our results herein indicate that wave properties such as shape and wave speed are very sensitive to release site distribution.

However, the observed wave shape is inconsistent with heterogeneous distribution of release sites and homogeneous diffusion. With release sites clustered along Z-lines and isotropic diffusion, we obtained highly elliptical waves. Countering the acceleration of wave velocity by the higher transverse release site density is the likely presence of barriers to transverse diffusion, such as mitochondria. The mitochondria constitute a significant portion of the cell volume. Page et al. (1971) employed electron microscopy to find that the mitochondria occupy 34% of a rat ventricular myocyte. From UV confocal images of NADH fluorescence, Cheng et al. (1996b) reported that the mitochondria are organized into highly ordered elongated bundles occupying ~30% of the cell. This suggests an increased tortuosity and reduced effective diffusivity for the calcium ion.

We confirmed quantitatively the reduction of transverse diffusion by microinjecting cardiac myocytes with the nonreactive dye fluorescein. We found that the transverse diffusion coefficient was 0.39 times that of the longitudinal diffusion coefficient, supporting the presence of transverse diffusion barriers. We found that the combination of release sites clustered at the Z-lines and a transverse diffusion coefficient 50% of that in the longitudinal direction generated waves of ellipticity 2/1 (major axis along the Z-line). The simulated waves generated with diffusion in the transverse direction were restricted to 50% and in the presence of intermediate release sites are in qualitative agreement with the experimentally observed waves. The evidence, in the form of the anisotropic fluorescein distribution and the diffusion barriers presented by subcellular organelles, therefore, provides strong support for restricted transverse diffusion.

Cellular organelles likely influence wave propagation in other ways besides passively restricting diffusion. In addition to functioning as diffusion barriers, mitochondria actively sequester and release calcium (Bassani et al. 1994; Gunter et. al., 1994; Szalai et al., 2000). Digital imaging of mitochondrial potentials reveals discrete, transient depolarizations, called flicker. Duchen et al. (1998) demonstrated that mitochondrial flicker was directly related to the focal release of calcium from the SR and consequent uptake by local mitochondria. Focal SR calcium release results in calcium microdomains sufficient to promote local mitochondrial calcium uptake, suggesting a tight coupling of calcium signaling between SR release and nearby mitochondria. We conducted preliminary experiments to elucidate the role of mitochondrial uptake upon wave shape. At normal conditions, mitochondria take up Ca^{2+} from the cytoplasm via a Ca^{2+} uniporter utilizing the negative membrane potential as driving force (Gunter and Pfeiffer, 1990; Bers, 1991). We added the mitochondrial Ca uptake inhibitor rotenone to the bathing solution (5 μM dissolved in DMSO). Rotenone increased the ellipticity of the waves in a direction parallel to the Z-lines. In the presence of this drug, the ratio of the transverse dimension to the longitudinal dimension increased from 0.94 ± 0.03 ($n = 47$) to 1.15 ± 0.02 ($n = 78$; $p < 0.001$). These data suggest that mitochondrial calcium uptake indeed partially influences wave shape. However, these data also suggest that active uptake alone cannot account for the longitudinal preference; otherwise highly elliptical waves such as those seen in Fig. 3 would result. On the basis of the relatively small distortion of the wave by inhibition of mitochondrial uptake, and the elongation of the fluorescein diffusion pattern in the longitudinal direction, it appears that transverse diffusion barriers must play a significant role in forming the shape of the wave.

It should be recalled that the combination of release sites localized on Z-lines and anisotropic diffusion did not yield

perfectly circular waves. We obtained essentially circular waves by introducing additional release sites between the Z-lines at a density 20% of that on the Z-lines produced. The experiments and simulations therefore support the presence of transverse diffusion barriers, and possibly intermediate release sites as well. This would suggest in turn a possible active role of the corbular SR, peripheral jSR and jSR-contacted axial tubules of transverse-axial tubular system in Ca^{2+} wave propagation. Some investigators have observed that longitudinal velocities are actually larger than transverse velocities (Engel et al., 1994). The presence of intermediate release sites would be consistent with this observation as well.

Although our model provides a basis for understanding the pattern of calcium waves, it has limitations. As noted previously, our simulations in Fig. 6 differed in several respects from our experiment in Fig. 2. Our simulated wave velocity (119 μm/s) was at the high end of the physiological range whereas the particular experiment in Fig. 2 features a wave velocity ($\sim$38 μm/s) near the lower end of the physiological range. The peak concentrations of Ca:dye in the simulation (17 μM) were half those of the experiment ($\sim$30 μM). We decided against a more extensive parameter fit to rigorously reproduce the experimental data after considering the insights presented by Keizer et al. (1998). These authors derived the following expression for the speed of a calcium wave from a single-dimension reaction diffusion equation with only discrete release terms (no uptake terms):

$$v = D/(d\bar{\Delta}(c^*,q_0)) \qquad (17)$$

The quantity v is the wave velocity, D is the diffusion coefficient, d is the release site spacing, and $\bar{\Delta}$ is the time interval of firing at two adjacent sites. The time interval is itself a nonlinear function of the source strength of the release site, q_0, and the firing threshold, c^*. Eq. 17 shows that the velocity is proportional to the diffusion coefficient, inversely proportional to the release site spacing, and dependent in a more complicated way upon firing threshold and source strength. The same qualitative behavior holds for the more complex system given by Eqs. 1–3, although the relationships are no longer linear and are not derivable analytically. There are rather large uncertainties in the accepted values of firing threshold and source strength, and the diffusion coefficient depends upon direction. Given the number of degrees of freedom, a parameter fit that rigorously reproduced the experiment would not establish the values of any of the parameters unambiguously and would be of little value.

The value of our model lies not in its ability to rigorously simulate a given experiment, but rather in its ability to illustrate the roles of diffusional anisotropy and release site distribution. These aspects of the cardiac myocyte are difficult to analyze with models that have closed-form solutions. Our model reconciles release site distribution with the spatial pattern of calcium waves, within the framework of diffusion-coupled calcium-induced calcium release. Diffusional asymmetry overlies release asymmetry, resulting in propagation symmetry of spherical waves. Spherical waves in turn permit contractile activation of the myocyte in a controlled and homogeneous manner.

To summarize, cellular ultrastructure exerts a significant influence upon the propagating characteristics of calcium waves in cardiac myocytes. This influence results from at least three factors: 1) reduction of transverse diffusion due to anisotropy of the myoplasm, 2) heterogeneous distribution of calcium release sites, and 3) heterogeneous distribution of active calcium uptake sites on mitochondria. Additional research is required to explore the roles of intermediate release sites and uptake by structures such as the cytoskeleton.

This work was supported by the National Institutes of Health (HL63043–01). S. Gyorke is an Established Investigator of the American Heart Association.

REFERENCES

Albritton, N. L., T. Meyer, and L. Stryer. 1992. Range of messenger action of calcium ion and inositol 1,4,5-trisphosphate. *Science.* 258: 1812–1815.

Balke, C. W., T. M. Egan, and W. G. Wier. 1994. Processes that remove calcium from the cytoplasm reticulum during excitation-contraction coupling in intact rat heart cells. *J. Physiol.* 474:447–472.

Bassani, R. A., J. W. M. Bassani, and D. M. Bers. 1994. Relaxation in ferret ventricular myocytes: unusual interplay among calcium transport systems. *J. Physiol.* 476:295–308.

Bers, D. M. 1991. Excitation-Contraction Coupling and Cardiac Contractile Force. Kluwer Academic Publishers, Dordrecht, The Netherlands.

Bugrim, A. E., M. R., Zhabotinsky, A. M., and I. R. Epstein,. 1997. Calcium waves in a model with a random spatially discrete distribution of Ca^{2+} release sites. *Biophys. J.* 73:2897–2906.

Carslaw, H., and G. Jaeger. 1959. Conduction of Heat in Solids, 2nd ed. Clarendon Press, Oxford. 256–258.

Cheng, H., M. B. Cannell, and W. J. Lederer. 1994. Propagation of excitation-contraction coupling into ventricular myocytes. *Pfluegers Arch.* 428:415–417.

Cheng, H., M. R. Lederer, W. J. Lederer, and M. B. Cannell. 1996a. Calcium sparks and $[Ca^{2+}]_i$ waves in cardiac myocytes. *Am. J. Physiol.* 270:C148–C159.

Cheng, H., M. R. Lederer, R. P. Xiao, A. M. Gomez, Y. Y. Zhou, B. Ziman, H. Spurgeon, E. G. Lakatta, and W. J. Lederer. 1996b. Excitation-contraction coupling in heart: new insights from Ca^{2+} sparks. *Cell Calcium.* 20:129–140.

Dawson, S. P., J. Keizer, and J. Pearson. 1999. Fire-diffuse-fire model of dynamics of intracellular calcium waves. *Proc. Nalt. Acad. Sci. U.S.A.* 96:6060–6063.

Deen, W. M. 1998. Analysis of Transport Phenomena. Oxford University Press. New York. 188–189.

Duchen, M. R., A. Leyssens, and M. Crompton. 1998. Transient mitochondrial depolarizations reflect focal sarcoplasmic reticular calcium release in single rat cardiomyocytes. J. *Cell Biol.*142: 975–988.

Engel, J., M. Fechner, A. J. Sowerby, S. A. E. Finch, and A. Stier. 1994. Anisotropic propagation of Ca^{2+} waves in isolated cardiac myocytes. *Biophys. J.* 66:1756–1762.

Engel, J., A. J. Sowerby, A. E. Finch, M. Fechner, and A. Stier. 1995. Temperature dependence of Ca^{2+} wave properties in cardiomyocytes: implications for the mechanism of autocatalytic Ca^{2+} release in wave propagation. *Biophys. J.* 68:40–45.

Escobar, A. L., F. Cifuentes, and J. L. Vergara. 1995. Detection of Ca^{2+}-transients elicited by flash photolysis of DM-nitrophen with a fast calcium indicator. *FEBS Lett.* 364:335–338.

Fabiato, A. 1983. Calcium-induced release of calcium from the cardiac sarcoplasmic reticulum. *Am. J. Physiol.* 245:C1–C14.

Failli, P., C. Ruocco, A. Fazzini, and A. Giotti. 1997. Calcium waves in unstimulated left ventricular cardiomyocytes isolated from aged spontaneously hypertensive and normotensive rats. *Biochem Biophys. Res. Commun.* 237:103–106.

Flucher, B. E., and C. Franzini-Armstrong. 1996. The path of calcium in cytosolic calcium oscillations: a unifying hypothesis. *Proc. Natl. Acad. Sci. U.S.A.* 88:9883–9887.

Forbes, M. S., and E. E. Van Niel. 1988. Membrane systems of guinea pig myocardium: ultrastructure and morphometric studies. *Anat. Rec.* 222: 362–379.

Franzini-Armstrong, C. 1996. Functional significance of membrane architecture in skeletal and cardiac muscle. *Soc. Gen. Physiol. Ser.* 51:3–18.

Franzini-Armstrong, C., and F. Protasi. 1997. Ryanodine receptors of striated muscles: a complex channel capable of multiple interactions. *Physio. Rev.* 77:699–729.

Franzini-Armstrong, C., F. Protasi, and V. Ramesh. 1999. Size, shape, and distribution of Ca^{2+} release units and couplons in skeletal and cardiac muscles. *Biophys. J.* 77:1528–1539.

Grouselle, M., B. Stuyvers, S. Bonoron-Adele, P. Besse, and D. Georges-cauld. 1991. Digital imaging microscopy analysis of calcium release from sarcoplasmic reticulum in single rat cardiac myocytes. *Pfluegers Arch.* 418:109–119.

Gunter, T. E., K. K. Gunter, S. S. Sheu, and C. E. Gavin. 1994. Mitochondrial calcium transport: physiological and pathological relevance. *Am. J. Physiol.* 267:C313–C319.

Gunter, T. E., and D. R. Pfeiffer. 1990. Mechanisms by which mitochondria transport calcium. *Am. J. Physiol.* 258:C755–C786.

Györke, S., V. Lukyanenko, and I. Györke. 1997. Dual effects of tetracaine on spontaneous calcium release in rat ventricular myocytes. *J. Physiol.* 500:297–309.

Hamill, O., A. Marty, E. Neher, B. Sakmann, and F. Sigworth. 1981. Improved patch-clamp techniques for high-resolution current recording from cells and cell-free membrane patches. *Pfluegers Arch.* 391:85–100.

Harkins, A. B., N. Kurebayashi, and S. M. Baylor. 1993. Resting myoplasmic free calcium in frog skeletal muscle fibers estimated with fluo-3. *Biophys. J.* 65:865–881.

Ishide, N., T. Urayama, K. I. Inoue, T. Komaru, and T. Takishma. 1990. Propagation and collision characteristics of calcium waves in rat myocytes. *Am. J. Physiol.* 259:H940–H950.

Izu, L. T., W. G. Wier, and C. W. Balke. 1998. Theoretical analysis of the Ca^{2+} spark amplitude distribution. *Biophys. J.* 75:1144–1162.

Jaffe, L. F. 1991.The path of calcium in cytosolic calcium oscillations: a unifying hypothesis. *Proc. Natl. Acad. Sci. U.S.A.* 88:9883–9887.

Jorgensen, A. O., A. C. Shen, W. Arnold, P. S. McPherson, and K. P. Campbell.1993. The Ca^{2+} release channel/ryanodine receptor is localized in junctional corbular sarcoplasmic reticulum in cardiac muscle. *J. Cell Biol.* 120:969–980.

Jorgensen, A. O., A. C. Shen, and K. P. Campbell. 1985. Ultrastructural localization of calsequestrin in adult rat atrial and ventricular muscle cells. *J. Cell Biol.* 101:257–268.

Kargacin, G. J. 1994. Calcium signaling in restricted diffusion spaces. *Biophys. J.* 67:262–272.

Keizer, J., and G. Smith. 1998. Spark to wave transition: saltatory transmission of calcium wave in cardiac myocytes. *Biophys. Chem.* 72:87–100.

Keizer, J., G. Smith, S. Ponce-Dawson, and J. Pearson. 1998. Saltatory propagation of Ca^{2+} waves by Ca^{2+}sparks. *Biophys. J.* 75:595–600.

Koch, C. 1999. The Biophysics of Computation. Oxford University Press, New York. 266–267.

Kupferman, R., P. Mitra, P. C. Hohenberg, and S. Wang. 1997. Analytical calculation of intracellular calcium wave characteristics. *Biophys. J.* 72:2430–2444.

Lakatta, E. 1992. Functional implications of spontaneous sarcoplasmic reticulum Ca^{2+} release in the heart. *Cardiovasc. Res.* 26:193–214.

Langer, G., and A. Peskoff. 1996. Calcium concentration and movement in the diadic cleft space of the cardiac ventricular cell. *Biophys. J.* 70: 1169–1182.

Lukyanenko, V., and S. Györke. 1999. Ca^{2+} sparks and Ca^{2+} waves in rat saponin-permeabilized ventricular myocytes. *J. Physiol.* 521:575–585.

Lukyanenko, V., S. Subramanian, I. Györke, T. F. Wiesner, and S. Györke. 1999. The role of lumenal Ca^{2+} in the generation of Ca^{2+} waves in rat ventricular myocytes. *J. Physiol.* 518:173–186.

Ogata, T., and Y. Yamasaki. 1993. Ultra-high resolution scanning electron microscopic studies on the sarcoplasmic reticulum and mitochondria in various muscles: a review. *Scanning Microsc.* 7:145–156.

Page, E., L. P. McCallister, and B. Power. 1971. Stereological measurements of cardiac ultrastructures implicated in excitation-contraction coupling. *Proc. Natl. Acad. Sci. U.S.A.* 68:1465–1466.

Parker, I., W. J. Zang, and W. G. Wier. 1996. Ca^{2+} sparks involving multiple Ca^{2+} release sites along Z-lines in rat heart cells. *J. Physiol.* 497:31–38.

Peskoff, A., and G. A. Langer. 1998. Calcium concentration and movement in the ventricular cardiac cell during an excitation-contraction cycle. *Biophys. J.* 74:153–174.

Pratusevich, V. R., and C. W. Balke. 1996. Factors shaping the confocal image of the calcium spark in cardiac muscle cells. *Biophys. J.* 71: 2942–2957.

Segall, N. L., and J. F. MacGregor. 1984. Collocation methods for solving packed bed reactor models with radial gradients. *Can. J. Chem. Eng.* 62:808–817.

Shacklock, P. S., W. G. Wier, and C. W. Balke. 1995. Local Ca^{2+} transients (Ca^{2+} sparks) originate at transverse tubules in rat heart cells. *J. Physiol.* 487:601–608.

Sipido, K. R., and W. G. Wier. 1991. Flux of Ca^{2+} across the sarcoplasmic reticulum of guinea-pig cardiac cells during excitation-contraction coupling. *J. Physiol.* 435:605–630.

Smith, G. D., J. E. Keizer, M. D. Stern, W. J. Lederer, and H. Cheng. 1998. A simple numerical model of calcium spark formation and detection in cardiac myocytes. *Biophys. J.* 75:15–32.

Stern, M. D. 1992. Theory of excitation contraction coupling in cardiac muscle. *Biophys. J.* 63:497–517.

Stern, M. D., M. C. Capogrossi, and E. G. Lakatta. 1988. Spontaneous calcium release from the sarcoplasmic reticulum in myocardial cells: mechanisms and consequences. *Cell Calcium.* 9:247–256.

Szalai, G., G. Csordas, B. M. Hantash, A. P. Thomas, and G. Hajinoczky. 2000. Calcium signal transmission between ryanodine receptors and mitochondria. *J. Biol. Chem.* 275:15305–15313.

Takahashi, A., and T. Takamatsu. 1997. Effects of basal $[Ca^{2+}]_i$ on calcium handling in Ca^{2+} overloaded rat cultured heart muscle cells. *Cell. Signal.* 9:617–625.

Takamatsu, T., and W. Wier. 1990. Calcium waves in mammalian heart: quantification of origin, magnitude, waveform, and velocity. *FASEB J.* 4:1519–1525.

Tang, Y., and H. G. Othmer. 1994. A model of calcium dynamics in cardiac myocytes based on the kinetics of ryanodine-sensitive calcium channels. *Biophys. J.* 67:2223–2235.

Trafford, A. W., P. Lipp, S. C. O'Neill, E. Niggli, and D. Eisner. 1995. Propagating calcium waves initiated by local caffeine application in rat ventricular myocytes. *J. Physiol.* 489:319–326.

Villadsen, J. V., and W. E. Stewart. 1967. Solution of boundary-value problems by orthogonal collocation. *Chem. Eng. Sci.* 22:1483–1501.

Wagner, J., and J. Keizer. 1994. Effects of rapid buffers on Ca^{2+} diffusion and Ca^{2+} oscillations. *Biophys. J.* 67:447–456.

Williams, D. A., L. M. Delbridge, S. H. Cody, P. J. Harris, and T. O. Morgan. 1992. Spontaneous and propagated calcium release in isolated cardiac myocytes viewed by confocal microscopy. *Am. J. Physiol.* 262:C731–C742.

Wussling, M. H., and H. Salz. 1996. Nonlinear propagation of spherical calcium waves in rat cardiac myocytes. *Biophys. J.* 70:1144–1153.

Wussling, M. H., K. Scheufler, S. Schmerling, and V. Drygalla. 1997. Velocity-curvature relationship of colliding spherical calcium waves in rat cardiac myocytes. *Biophys. J.* 73:1232–1242.

Yao, Y., J. Choi, and I. Parker. 1995. Quantal puffs of intracellular Ca^{2+} evoked by inositol trisphosphate in *Xenopus* oocytes. *J. Physiol.* 482: 533–553.